JOURNAL OF SOLID STATE CHEMISTRY **126,** 7–14 (1996)
ARTICLE NO. 0302

Thermal Behavior and Cation Distribution of Submicron Copper Ferrite Spinels $Cu_xFe_{3-x}O_4$ ($0 \leq x \leq 0.5$) Studied by DTG, FTIR, and XPS

E. Kester, B. Gillot, P. Perriat, and Ph. Dufour

Laboratoire de Recherche sur la Réactivité des Solides, URA CNRS and 23 Faculté des Sciences Mirande, B.P. 138, 21004 Dijon Cedex, France

C. Villette, Ph. Tailhades, and A. Rousset

Laboratoire de Chimie des Matériaux Inorganiques, URA CNRS 1311, Université Paul Sabatier 118, route de Narbonne, 31062 Toulouse Cedex, France

Received January 22, 1996; in revised form May 20, 1996; accepted May 28, 1996

The valence state and the cation distribution on octahedral (B) and tetrahedral (A) sites in the spinel structure of Cu and Fe ions has been determined in nanometric copper-substituted magnetites, $Cu_xFe_{3-x}O_4$ ($0 \leq x \leq 0.5$), by TG, DTG, FTIR, and XPS. The oxidation of the oxidizable cations has also been investigated: It was demonstrated that Cu_B^+, Fe_B^{2+}, and Cu_A^+ oxidize into Cu^{2+} and Fe^{3+} ions below 300°C. Moreover, the stability of each cation toward oxidation, decreasing from Cu_B^+ to Cu_A^+, has been found in close relation with the cation–oxygen distance of each oxidizable cation. A quantitative analysis by DTG based on this difference of reactivity only permits one to determine the concentration of B-site (Fe^{2+} + Cu^+) ions and A-site Cu^+ ions. Using TG analysis performed on different experiments varying the oxygen partial pressure, the cationic distribution has been obtained. It is given by the formula

$$(Cu^+_{\alpha x}Fe^{3+}_{1-\alpha x})_A(Cu^{3+}_{(1-\alpha-\beta)x}Cu^+_{\beta x}Fe^{3+}_{1+(2\alpha+\beta)x}Fe^{2+}_{1-(1+\alpha+\beta)x})_BO^{2-}_4,$$

where α and β varies with x. $\alpha = 0.50$ and $\beta = 0.20$ for $x = 0.32$. From FTIR and XPS data, it has been shown that when the deviation from stoichiometry is the greatest the vacancies and all the Cu^{2+} ions are on B-sites.

1. INTRODUCTION

In previous studies (1–3), it has been demonstrated that in nanometric transition metal oxides with spinal structure, the cationic distribution between the tetrahedral (A) and octahedral (B) site sublattices can be accurately determined from a quantitative analysis by derivative thermogravimetry (DTG) of oxidizable cations. Determination of the cation distribution in stoichiometric $M_xFe_{3-x}O_4$ (M = Mn, Mo, V) and in spinels with a deviation from stoichiometry, $M_xFe_{3-x}O_{4+\delta}$ (γ-phases), are of considerable interest in solid state chemistry because they may allow investigation of the relative stabilities of the metal ions in A, and B-sites and better understanding of the correlations between structure and some properties such as coercivity (magnetic recording) (4), electrical conductivity (electronic industry) (5, 6), catalytic activity (CO oxidation) (7, 8), etc., which are well known to be quite dependent on the relative A-, and B-site occupancy by transition metal ions.

This paper is one of a series which describes an investigation of the relation between the structure and some variables such as temperature, composition, and oxygen partial pressure in spinel-type oxides formed in the Cu–Fe–O system obtained by a wet procedure. Concerning $CuFe_2O_4$, there have been very extensive studies (9–11) of the oxidation states of copper and its distribution in both cubic and tetragonal spinel-types which are sensitive to the synthesis procedures, oxygen pressure, and heat treatment. For example, it has been shown that the electron exchange between Cu and Fe, $Cu_A^{2+} + Fe_B^{3+} = Cu_B^{2+} + Fe_A^{3+}$ becomes significant above 200°C and that a reoxidation of Cu^+ ions formed above 600°C is involved near 325°C (10).

In this work, the cation distribution in submicron $Cu_xFe_{3-x}O_4$ solid solutions ($0 \leq x \leq 0.5$) has been studied by thermogravimetry (TG and DTG), X-ray diffraction, FTIR spectroscopy, and XPS. We describe the combined use of the four techniques to evaluate the valence and copper ion distribution and its dependence on temperature and oxygen partial pressure. For this composition range, only qualitative distributions have been proposed owing to the difficulty of obtaining submicron copper ferrites (12) that has so far precluded a quantitative analysis.

0022-4596/96 $18.00

2. EXPERIMENTAL

2.1 Samples

$Cu_xFe_{3-x}O_4$ particles with an acicular shape (acicular ratio around 4.5) were prepared by a "chimie douce" method via decomposition of mixed oxalate precursors as reported in Ref. (12). The mixed oxalates $Cu_{(1-x)}/Fe_{2/3}C_2O_4,2H_2O$ were first decomposed under air flow at 250°C and then annealed at 600°C. After this treatment, three phases are present: α-Fe_2O_3, CuO, and $CuFe_2O_4$. The single-spinel phases were obtained by further annealing between 160 and 290°C of $N_2/H_2/H_2O$ mixtures. The spinel formation was checked by X-ray diffraction using Co$K\alpha$ radiation and the average crystallite size measured from the X-ray lines broadening was close to 30 nm. This technique was also used to determine the lattice parameter by using rock salt (NaCl) as internal reference.

2.2. Measurements

The oxidation and reduction reactions were performed in a Setaram MTB 10-8 microbalance (symmetrical setup, resolution and noise level ~0.1 μg) with the temperature increasing at a linear rate (2°C min^{-1}) or under isothermal conditions. The material weighed 10 mg and the powder was spread out so that it would oxidize in the same way as independent particles of equal mean radius.

The infrared spectra were recorded with a Perkin–Elmer 1725× FTIR spectrometer over the range 4000–400 cm^{-1} and with a Perkin–Elmer 1700 FTIR over the range 500–50 cm^{-1}. One milligram of sample was mixed with 200 mg of spectroscopically pure dry Csl and pressed into disks before the spectra were recorded.

X-ray photoelectron spectroscopy (XPS) results were obtained with a Riber spectrometer AES-ESCA-ELS MAG2 instrument equipped with an Al anode operating at 13 kV and 20 mA current emission ($h\nu$ = 1486.6 eV). Binding energies were determined from a *C*1*s* peak at 285 eV, and the ferrite powder was pressed into a piece of indium foil (99.999%) that was grounded to the spectrometer in the examination.

The differential scanning calorimetry (DSC) experiments were carried out under air with a Setaram DSC 111G. These measurements were made with about 60 mg of powder.

3. RESULTS AND DISCUSSION

3.1 Thermal Behavior under a Pure Oxygen Pressure of 4 × 10^3 Pa

In Fig. 1a, the TG curves between room temperature and 1200°C evidence two domains. In a first temperature range (region I) a mass gain is observed on heating. This gain originates above 100°C and reaches a maximum near

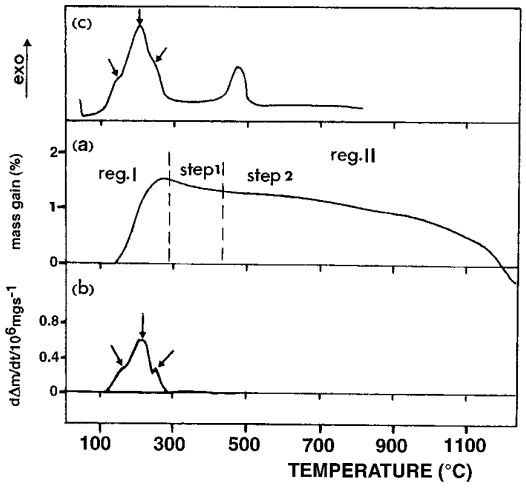

FIG. 1. Thermal behavior curves of a $Cu_xFe_{3-x}O_4$ spinel in O_2 at 4 × 10^3 Pa: (a) TG, (b) DTG, (c) DSC.

300°C. In a second range beyond 300°C (region II) a discontinuous mass loss is detected. As revealed from the DTG and DSC curves (Figs. 1b and 1c), in region I where the spinal structure is preserved, as seen in X-ray diffraction, a main peak located near 200°C and two shoulders at about 160 and 250°C can be observed. Therefore, in this small temperature range, three cations are involved in the oxidation mechanism, characterized by the overall raction:

$$(Cu, Fe)_3O_4 + \delta_1/4O_2 \rightarrow (Cu, Fe)_3O_{4+\delta_1}. \qquad [1]$$

During this reaction, the experimental lattice parameter progressively decreases (Fig. 2, curve a), which is consistent with the oxidation of iron and copper ions.

A careful examination of the loss mass in region II (curve a) reveals that the reduction process has a two-step character. In the temperature range 300–450°C, where the spinel structure was also preserved (step 1), the sharp loss mass is not accompanied by any thermal effect in the DSC curve (curve c). This can be explained, again, by the variation of the cation/vacancy ratio in the spinel structure according to the reaction:

$$(Cu, Fe)_3O_{4+\delta_1} \rightarrow (Cu, Fe)_3O_{4+\delta_2} + (\delta_1 - \delta_2)/4O_2. \qquad [2]$$

Since in other Fe-based spinels, Fe^{3+} is thermodynamically stable under air up to 800°C, reaction (2) can be relative to the reduction of Cu^{2+} to Cu^{+}. This reduction is accompanied by a low increase of lattice constant (Fig. 2, curve a).

Above 450°C, the mass loss in the second step takes place with phase transformation as shown by the exothermic peak (curve c) located around 490°C. X-ray diffraction

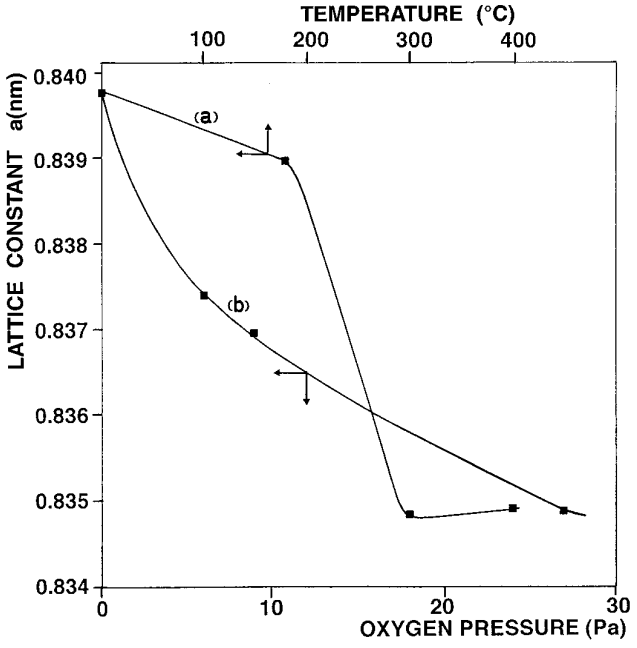

FIG. 2. Variation of lattice constant (1) for $Cu_{0.32}Fe_{2.68}O_4$ spinel (a) with oxidation temperature, (b) with oxygen pressure.

studies indicate that the formed phases are α-Fe_2O_3 and a spinal phase, and, considering that the excess of oxygen measured in region T is not totally removed, the following reaction can be written:

$$(Cu, Fe)_3O_{4+\delta_2} \rightarrow \alpha\text{-}Fe_2O_3 + (Cu, Fe)_3O_4 + O_2. \quad [3]$$

The variation of the transition temperature $\gamma \rightarrow \alpha$ with the composition of the spinal shows an increase in the stability of the γ-phase when there is an increase the copper content (Fig. 3). Such an observation is consistent with the effect of divalent cations on the stabilization $\gamma \rightarrow \alpha$ transition of γ-Fe_2O_3, as already reported (13, 14).

When the temperature becomes higher than 600°C, the amount of precipitated α-ferric oxide decreases, this precipitation disappearing completely at about 1200°C, leading to a stoichiometric spinel phase (15).

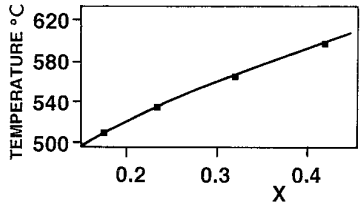

FIG. 3. Effect of copper content (x) on temperature of precipitation.

3.2. Cationic Distribution

3.2.1. Approach from Lattice Constant

The lattice parameter (a) of the $Cu_xFe_{3-x}O_4$ spinels increases with the copper content (x) (Fig. 4, curve a) and the S-shaped curves is a direct consequence of the cation distribution. In order to explain this variation and to try to determine the cation distribution, theoretical $a = (f(x)$ curves were calculated for different structural formula by considering, on the one hand, the substitution of iron by both Cu^+ and Cu^{2+} ions in each A-, and B-site, and on the other hand, by taking into account various representative distributions proposed by several authors (12, 16–18). The substitution of iron by copper was therefore made according to the following structural formulas where the fourfold and sixfold Cu^+ and Cu^{2+} ions coordinations were considered:

$$(Fe^{3+})_A\,(Cu_x^{2+}Fe_{1-x}^{2+}Fe^{3+})_B O_4^{2-} \quad [4]$$

$$(Cu_x^{2+}Fe_{1-x}^{3+})_A\,(Fe_{1-x}^{2+}Fe_{1+x}^{3+})_B O_4^{2-} \quad [5]$$

$$(Fe^{3+})_A\,(Cu_x^{+}Fe_{1-2x}^{2+}Fe_{1-x}^{3+})_B O_4^{2-} \quad [6]$$

$$(Cu_x^{+}Fe_{1-x}^{3+})_A\,(Fe_{1-2x}^{2+}Fe_{1+2x}^{3+})_B O_4^{2-} \quad [7]$$

$$(Cu_{0.5x}^{2+}Fe_{1-0.5x}^{3+})_A\,(Cu_{0.5x}^{2+}Fe_{1-x}^{2+}Fe_{1+0.5x}^{3+})_B O_4^{2-} \quad [8]$$

$$(Cu_{0.5x}^{+}Fe_{1-0.5x}^{3+})_A\,(Cu_{0.5x}^{2+}Fe_{1+x}^{3+}Fe_{1-1.5x}^{2+})_B O_4^{2-} \quad [9]$$

$$(Cu_{0.5x}^{+}Fe_{1-0.5x}^{3+})_A\,(Cu_{0.2x}^{+}Cu_{0.3x}^{2+}Fe_{1-1.7x}^{2+}Fe_{1+1.2x}^{3+})_B O_4^{2-}. \quad [10]$$

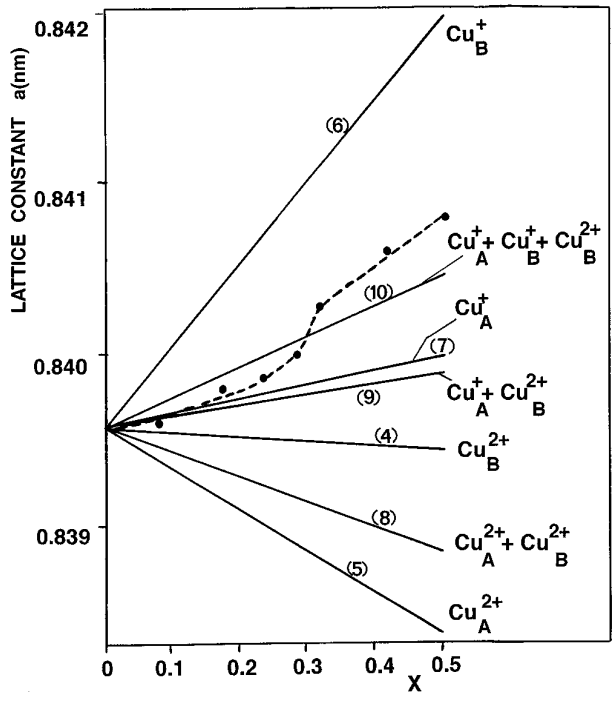

FIG. 4. Lattice constant (a) of $Cu_xFe_{3-x}O_4$ spinel ferrites versus copper content (x). Experimental points (●) and calculated curves assuming the structural formulas [4], [5], [6], [7], [8], [9], and [10].

TABLE 1
The "Cation–Anion" Distance in A- and B-sites of Cubic Spinels for Iron and Copper

Anion–cation bonds	B-site (nm)	A-site (nm)
Fe^{2+}–O	0.2132	0.2003
Fe^{3+}–O	0.2020	0.1858
Cu^{2+}–O	0.2130	0.1940
Cu^{+}–O	0.2282	0.2070
		0.2086

Lattice constants were calculated using the equations developed by Poix (19, 20) and based on the invariant character of metal–oxygen distances listed in Table 1. The Cu–O distances were derived from Refs. (21, 22).

As shown in Fig. 4, the calculated curves for the [4], [5], and [8] distributions have a slope opposite to that of the experimental curve, revealing that these three formulas are unable to describe the cation distribution. The [6] distribution with only Cu^{+} ions on B sites also exhibits a strong difference from experimental lattice constant values. The agreement is better for [9] and [7] distributions on the assumption that Cu^{+} ions are located on A-sites, but only for $x < 0.30$. In summary, it is concluded that a distribution with Cu^{2+} ions on B-sites and Cu^{+} ions on A- and B-sites gives a better agreement. The last formula tested (curve 10) confirms this point of view. However, it should be pointed out that, because of the S-shaped curve of the lattice constant vs composition, the relative content of Cu^{+} on A- and B-sites does not vary linearly with the Cu content.

Therefore, in a first approach a general chemical formula for copper ferrites can be proposed by also taking into account the presence of Fe^{2+} and Fe^{3+} ions on both sites:

$$(Cu^{+}_{\alpha x} Fe^{2+}_{\gamma x} Fe^{3+}_{1-\alpha x-\gamma x})_A \; (Cu^{+}_{\beta x} Cu^{2+}_{(1-\alpha-\beta)x} Fe^{2+}_{1-(1+\alpha+\beta-\gamma)x} Fe^{3+}_{1+(2\alpha+\beta-\gamma)x})_B \; O^{2-}_4. \quad [11]$$

A more detailed study of this distribution has been made by thermogravimetric analysis in order to determine the distribution parameters, α, β, and γ and the dependence of these parameters on the Cu content.

3.2.2. Study by Thermogravimetry

3.2.2.1. Qualitative analysis. It has been previously established that the oxidation temperature of M^{n+} ions located on B sites is lower than that of the M^{n+} ions located on A sites because of the weaker ionic bonding of the B-sites as compared with the stronger A-site covalent bonds (23). In this context an analysis by thermogravimetry on the basis of a redox-type mechanism of copper has been attempted to differentiate the oxidation temperature of each oxidizable cation. Figure 5 (curve a) shows the DTG curve for a sample with $x = 0.32$. As previously stated, three oxidations should be implicated with this temperature resolution. The intense peak at 200°C can be attributed unambiguously to the B-site Fe^{2+} ion oxidation, this oxidation temperature having been largely demonstrated elsewhere (1, 2) in other Fe-based spinels with the same particle size. The presence of Fe^{2+} ions on A-sites should be rule out owing to the oxidation temperature of these ions (420°C) for spinels having the same crystallite size and containing only Fe^{2+} ions on A-sites (24). From these considerations the γ coefficient of Eq. (11) is equal to zero and the peak at 290°C and the shoulder at 150°C represent only some oxidation of the copper ions.

For manganite spinels $Cu_xMn_{3-x}O_4$ ($0 < x < 1$) synthetized from coprecipitated hydroxide precursors and containing A-site Cu^{+} ions, studies made on cation distribution (25) have established that the low-temperature oxidation step starting at 300°C and extending up to a maximum of around 380°C is principally due to the oxidation of Cu^{+} ions located on A-sites. From this comparison, it is possible to attribute, in copper ferrites, the peak appearing at 290°C to the oxidation of Cu^{+}_A ions. The shoulder appearing at about 150°C may be relative to the oxidation of B-site Cu^{+} ions, this assumption being supported by its larger cation–oxygen distance (Table 1). To our knowledge this is the first well-documented example proving that the oxidation temperature of a such cation is lower than that of Fe^{2+} ions, both cations being located at B-sites.

3.2.2.2. Quantitative analysis. In order to propose a cationic distribution, a quantitative analysis of the cation from the determination of oxiation peak areas has been investigated. Due to first the accuracy of the balance and second the precision of the method of desummation, the content

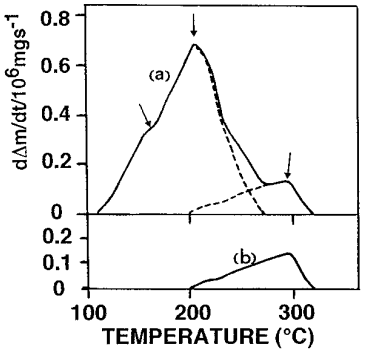

FIG. 5. DTG curves $d\Delta m/dt = f(T)$. (a) Oxidation global curve and desummation peaks, (b) curve showing the disappearance of the first (Cu^{+}_B) and second (Fe^{2}_B) oxidation after selective oxidation at 140°C for 24 h at $PO_2 = 4 \times 10^3$ Pa.

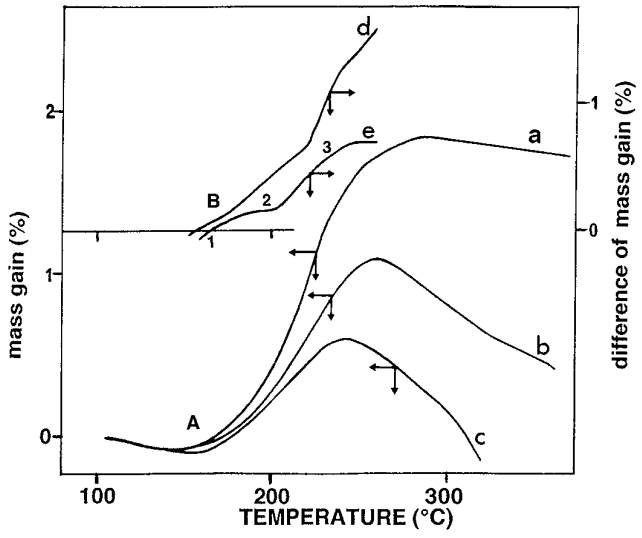

FIG. 6. TG curves for $Cu_{0.32}Fe_{2.68}O_4$ spinel: (A) for various oxygen pressures, (a) 27, (b) 9, (c) 6 Pa; (B) difference of mass gain, (d) 27 − 9, (e) 27 − 6 Pa.

of each oxidizable cation can be obtained with a relative accuracy better than 2%. The profile of the peak attributed to the oxidation of Cu^+ ions on A-sites, first determined by desummation (Fig. 5, curve a), has been confirmed by DTG after selective oxidation in isothermal conditions at 140°C for 24 h of Cu^+ and Fe^{2+} ions on B-sites. After this procedure, the reoxidation on heating in O_2 corresponding to the curve b represents only the oxidation of Cu^+ ions on A-sites. Therefore, it would be possible to calculate from the peak area the α coefficient of Eq. [11]. However, since the temperatures of oxidation of Cu^+ and Fe^{2+} ions on B-sites are too close, it is not possible to separate with enough accuracy the two oxidation peaks relative to these two cations.

Since Cu ions do not oxidize at low oxygen pressure, the Cu^+ ion concentration on B-sites has been determined from oxygen loss when varying the oxygen pressure. Figure 6A shows the TG curves for different oxygen pressures. At 27 Pa and above (curve a) the cations Cu_B^+, Fe_B^{2+}, and Cu_A^+ are almost completely oxidized, as confirmed by the lattice constant value found to be the lowest (Fig. 2, curve b). The heating curves for 9 (curve b), and 6 Pa (curve c) show that the copper ion concentration is oxygen pressure dependent. Thereby the magnitude of the mass–gain difference between 27 Pa and lower partial pressures of oxygen corresponds to cations which have not been oxidized. The d and e curves of Fig. 6B show how this difference varies with temperature. The difference in oxygen content for curve e reaches a plateau region (marked 2) in the interval $180° < T < 205°C$, which corresponds to the almost complete oxidation of the Fe^{2+} ions. The magnitude of this difference can thus be attributed to the amount of $Cu_B^+ + Cu_A^+$ ions initially present in the spinel lattice. For an oxygen pressure of 6 Pa (curve d), the plateau region was absent. Therefore a significant amount of Fe_B^{2+} remains to be oxidized above 205°C, which is consistent with an oxidation mechanism that is strongly slowed down because of the decrease of the oxygen transport in the gas phase, directly dependent on PO_2. Quantitative interpretation of these data allows evaluation of the α and β coefficients of Eq. [11]. For $x = 0.32$ these coefficients are 0.50 and 0.20, respectively, with a relative accuracy better than 2%.

3.3. Distribution in Cation Deficient Spinels

As these copper ferrites may be oxidized at low temperature (Fig. 7), giving nonstoichiometric $Cu_xFe_{3-x}O_{4+\delta}$ spinels, a comparison of the cation distributions will be made with stoichiometric phases. This comparison was made using X-ray photoelectron spectroscopy to characterize the location of copper(I) and copper(II) and infrared spectroscopy to determine the location of vacancies.

The FTIR and XPS spectra of an unoxidized sample with $x = 0.32$ are shown in Figs. 8 and 9, respectively. When the copper is substituted for iron in Fe_3O_4 in FTIR spectrum exhibits two broad absorption bands near 353 and 562 cm^{-1} (Fig. 8, curve a), typical of a "chemical" disorder resulting from having Fe^{2+} and Fe^{3+} ions on equivalent sites (26, 27). The Cu 2*p*3/2 spectrum shows an intense peak at 932 eV (Fig. 9, curve a). It has a large value of the full width at half maximum (FWHM = 3.7 eV) compared with those of oxidized samples (Fig. 9, curves b and c), which seems to be a strong evidence for the presence of Cu in different binding states. As a matter of fact, the Cu 2*p*3/2 peak contains several signals whose binding energies have the following values: 930.7, 932, and 934 eV. Lenglet *et al.* (28) reported from the investigation of different Cu spinels the binding energy values for the different Cu species, Cu_B^{2+} 931.3 eV, Cu_A^+ 932.8 eV, Cu_B^{2+} 934 eV, Cu_A^{2+} 936.2 eV, and more recently Töpfer *et al.* (29) recorded the Cu2*p* spectrum of Cu–Ni manganite spinels and have attributed signals at 932 eV to Cu_A^+ and at 934 eV to Cu_B^{2+}. Note also that a low binding energy for Cu^+ (930.7 eV) has been found in ferrites and chromites

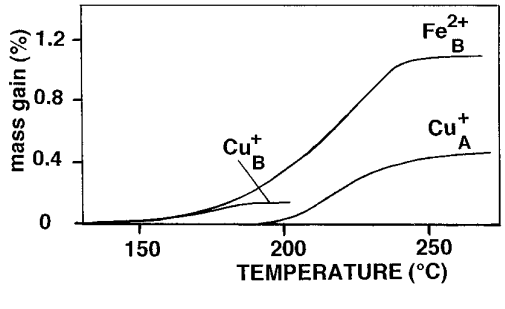

FIG. 7. Elementary oxidation curves for Cu_B^+, Fe_B^{2+}, and Cu_A^+.

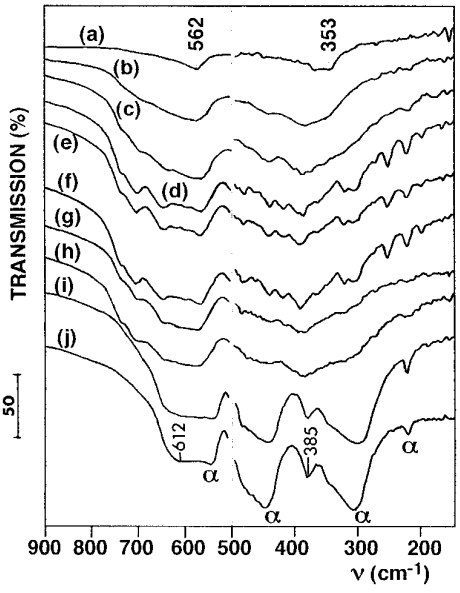

FIG. 8. FTIR spectra for a spinel with $x = 0.32$ oxidized under $PO_2 = 4 \times 10^3$ Pa at different temperatures. Each curve corresponds to an oxidation with the temperature increasing at a linear rate of 2°C min^{-1} and then quenched. (a) Initial, (b) 150, (c) 180, (d) 250, (e) 300, (f) 340, (g) 400, (h) 450, (i) 580, and (j) 650°C.

in octahedral symmetry (30, 31). In comparison with these results, the peak at 934 eV in the spectrum can be interpreted as belonging to Cu^{2+} on B-sites, the peak at 932 eV to Cu^{+} on A-sites, and at 931.3 eV to Cu^{+} on B-sites.

The FTIR spectra of oxidized samples under nonisothermal conditions ($PO_2 = 4 \times 10^3$ Pa, 2°C min^{-1}) and quenched from various temperatures are shown in Fig. 8 (curves b–j). In the temperature range 150–450°C (curves c–h) when cation-deficient spinels are formed, the spectra exhibit a large number of absorption bands, those being well resolved for samples oxidized at 250, 300, and 340°C (curves d, e, and f). For these three temperatures, the similarity with the FTIR spectrum of ordered γ-Fe_2O_3 (26), both in the position and number (at least 20) of absorption bands, permits us to postulate the same type of order between vacancies and cations on B-sites, i.e., a □/cation ratio of 1/5. Indeed, the complete oxidation of Cu_B^+, Fe_B^{2+}, and Cu_A^+ ions leads to a maximum of vacancy content. For $x = 0.32$, the number of vacancy approaches 0.24 per molecule (0.33 for γ-Fe_2O_3), and with vacancies on B-sites, a □/cation ratio of 0.14 is determined. For this ordered structure with a lower vacancy content than γ-Fe_2O_3, it was subsequently suggested that some ordering schemes may be adopted depending principally on the crystallite size and shape and also the mechanism of formation of the maghemite (32). Recently, we have shown from high-resolution electron microscopy (33) that the vacancy ordering in the oxidation product at low temperature of a zinc-substituted magnetite may be maintained if the Zn-content does not exceed 0.23, leading to a □/cation ratio of 0.15. This has been interpreted through the development of octahedral vacancy clusters.

For the same composition, the spinel oxidized at 180 and 450°C (curves c and h) shows the disappearance of some absorption bands, especially in the region 500–150 cm^{-1}. The observed difference may be reasonably explained by a lower number of vacancies resulting from only a partial oxidation of cations. It should be noted that at 180°C, only Cu_B^+ and some Fe_B^{2+} ions are oxidized, which strongly reduces the number of vacancies (around 0.18 per molecule), and therefore only a partial ordering occurs (26). The low vacancy content is confirmed by the larger value of the lattice constant (Fig. 2, curve a) compared to

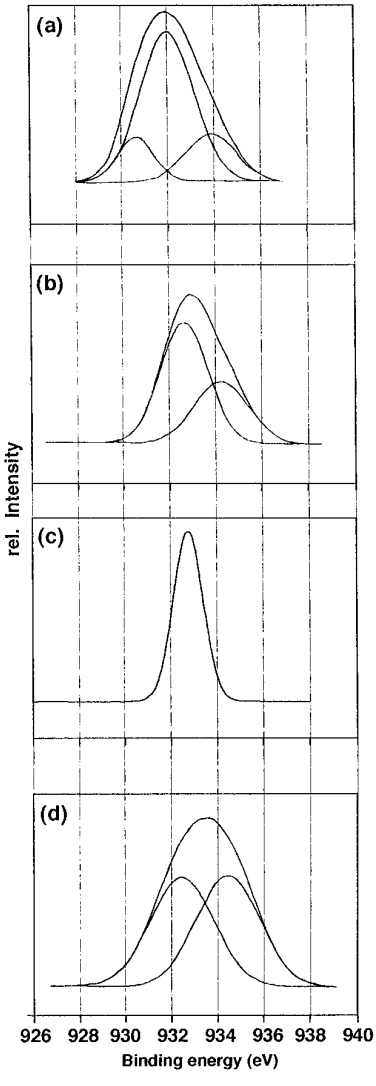

FIG. 9. Cu 2*p* core level spectra of a spinel with $x = 0.32$ (same treatment conditions as in Fig. 8): (a) initial, (b) 180, (c) 300, and (d) 400°C.

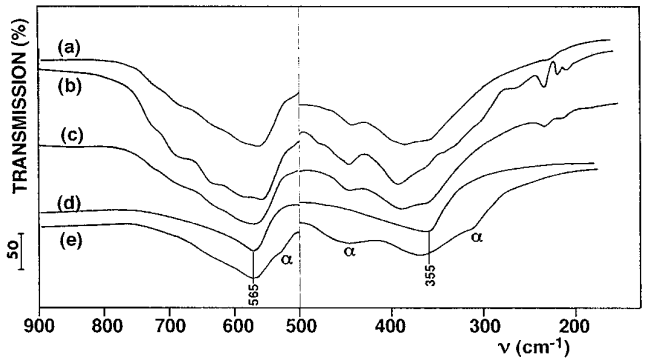

FIG. 10. FTIR spectra for a spinel with $x = 0.32$ oxidized under $PO_2 = 10$ Pa at different temperatures: (a) 230, (b) 250, (c) 270, (d) 400, and (e) 500°C.

a totally oxidized sample. On the other hand at 450°C, the decrease of vacancy content is related to the reduction of some cations occurring at this temperature. Moreover, the thermal agitation causes the randomness of vacancies on these sites. Beyond 500°C (Fig. 8, curves i and j), metastable cation-deficient spinels precipitate in two phases, α-Fe_2O_3 and a stoichiometric spinel, which are easily detectable in the FTIR spectrum by the presence of absorption bands at 230, 315, 450, 525 cm^{-1} characteristic of α-Fe_2O_3 (26) and at 385 and 612 cm^{-1} due to the spinel phase.

A qualitative inspection of a Cu $2p3/2$ spectrum of a sample oxidized at 180°C (Fig. 9, curve b) shows a Cu $2p3/2$ signal with a small FWHM value (3.1 eV) due to the absence of Cu_B^+ in the structure. Curve fitting yields only two signals caused by Cu^+ on A-sites (932.3 eV) and Cu^{2+} on B-sites (943.3 eV). With increasing temperature, more and more Cu ions are located as Cu^{2+} on B-sites, and at 300°C, where the mass gain is maximum, the signal is solely caused by Cu^{2+} ions on these sites (Fig. 9, curve c). The existence of an intense satellite peak at 944 eV in the spectrum clearly proved the presence of Cu^{2+} ions (34). It should be pointed out that the oxidation of Cu_A^+ is accompanied by its migration from A to B-sites since the signal at 936 eV characteristic of Cu^{2+} on A-sites can not be observed. This is in agreement with a consideration of the ligand field energies which predict a preference of Cu^{2+} ions for octahedral coordination (35). In the reduction temperature range where the spinel structure was maintained, some of the Cu^{2+} cations are reduced and the signal of Cu^+ on A-sites again appears (Fig. 9, curve d).

The comparison of the above results with samples heated in O_2 at 10 Pa and quenched at various temperatures was made from Figs. 10 and 11. The FTIR spectra (Fig. 10) recorded at several temperatures exhibit some bands and shoulders of low intensity in the frequency region 500–150 cm^{-1}, which can be corroborated by the fact that this oxygen pressure solely Fe^{2+} ions are oxidized. For example at 250°C (Fig. 10, curve c), where the number of vacancies per molecule approaches 0.15, the ordering between cations and vacancy is only partial and the spectrum presents a general similarity to that of samples treated under higher oxygen pressure but at a lower temperature (Fig. 8, curve c). At this low oxygen pressure, the initial spinel structure always predominates as evidenced by the presence of two broad absorption bands around 355 and 565 cm^{-1} (curves a–e). However, although at 400°C, the spinel returns to stoichiometry, the cation distribution differs owing to the fact that at this temperature the Cu^+ ions are absent on B-sites. Concerning the Cu $2p3/2$ peak, we found, after peak deconvolution, at least two components (Fig. 11). From the position of the peak on the binding energy scale it is clear that the peaks at ca. 934.4 (curve a) and 934.1 eV (curve b) are assigned to Cu^{2+} species on B-sites while the lower binding energy peaks at 932.3 (curve a) and 932.1 eV (curve b) are due to Cu^+ on A-sites. It can also be noted in Fig. 11 that the relative proportion of Cu^{2+} is higher in the sample treated at 300°C than in the sample treated at 270°C. However, no attempt has been made to obtain the percentage of Cu^+ and Cu^{2+} species from curve-fitting analysis.

From the reported investigations, oxidation of Cu^+ and Fe^{2+} ions on B-sites and Cu^+ ions on A-sites proceeds via the general reactions [12], [14], [16] in Kröger and Vink's notation (36), leading to the cation distributions [13], [15], and [17], where the distinction was made between cations

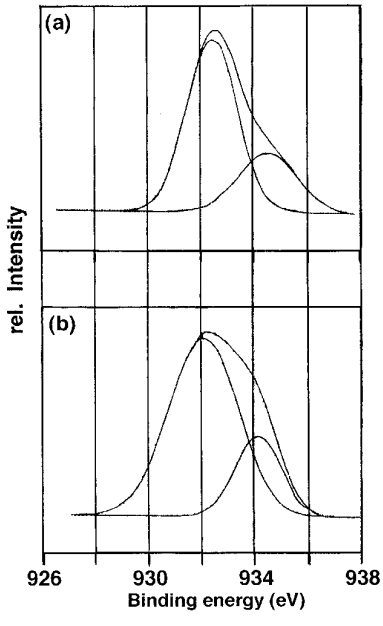

FIG. 11. Cu $2p$ core level spectra of a spinel with $x = 0.32$ oxidized under $PO_2 = 10$ Pa: (a) 270, (b) 300°C.

and vacancies on A- and B-sites according to the writing formalism defined in (37).

Oxidation of Cu^{+} ions on B-sites:

$$Cu_B^{+} + \tfrac{1}{8}\,Fe_B^{3+} + \tfrac{1}{4}\,O_2 \Rightarrow Cu_B^{2+} + \tfrac{1}{8}\,Fe_A^{3+} + \tfrac{3}{8}\,V_B + \tfrac{1}{2}\,O^{2-} \quad [12]$$

$$(Cu_{0.159}^{+}Fe_{0.841}^{3+})_A\,(Cu_{0.159}^{2+}Fe_{0.452}^{2+}Fe_{1.365}^{3+}\square_{0.024})_B\,O_4^{2-}. \quad [13]$$

Oxidation of Fe^{2+} ions on B-sites:

$$Fe_B^{2+} + \tfrac{1}{4}\,O_2 \Rightarrow \tfrac{7}{8}\,Fe_B^{3+} + \tfrac{1}{8}\,Fe_A^{3+} + \tfrac{3}{8}\,V_B + \tfrac{1}{2}\,O^{2-} \quad [14]$$

$$(Cu_{0.15}^{+}Fe_{0.85}^{3+})_A\,(Cu_{0.15}^{2+}Fe_{1.665}^{3+}\square_{0.185})_B\,O_4^{2-}. \quad [15]$$

Oxidation of Cu^{+} ions on A-sites:

$$Cu_A^{+} + \tfrac{9}{8}\,Fe_B^{3+} + \tfrac{1}{4}\,O_2 \Rightarrow Cu_B^{2+} + \tfrac{9}{8}\,Fe_A^{3+} + \tfrac{3}{8}\,V_B + \tfrac{1}{2}\,O^{2-} \quad [16]$$

$$(Fe^{3+})_A\,(Cu_{0.294}^{2+}Fe_{1.468}^{3+}\square_{0.238})_B\,O_4^{2-}. \quad [17]$$

4. CONCLUSION

These results show that submicron $Cu_xFe_{3-x}O_4$ particles ($0 < x$ 0.50) with an acicular shape and prepared from oxalic precursors are highly reactive with oxygen. Consequently, because of their small crystallite size, these ferrite particles can oxidize below 300°C, giving cation-deficient spinels. The DTG and DSC curves exhibit three oxidation stages, each oxidation being closely related to the cation–oxygen distance of each oxidizable cation. Thus, the Cu^{+} ions on B-sites with a cation–oxygen distance of 0.2282 nm oxidize, at a lower temperature (150°C) than the Fe^{2+} ions on B-sites (200°C) having a cation–oxygen distance of 0.2132 nm, whereas the Cu^{+} ions on A-sites with a cation–oxygen distance around 0.208 nm oxidize above 250°C. In connection with this, a quantitative analysis by DTG and TG based on this difference of reactivity permits, for $x = 0.32$, the proposal of a cation distribution between the A and B sublattices of the spinel structure. However, the S-shaped curve of the lattice constant significantly alters a generalization of the results for the entire composition range.

We have also demonstrated that spectroscopic methods such as FTIR and XPS can give fine information on cation-deficient spinels. In particular, the FTIR spectra of samples oxidized at 300°C provide evidence for the location of vacancies on B-sites with an ordering on these sites in which a large number of absorption bands are present. XPS is very sensitive to location and oxidation states of copper. The oxidation state change of Cu from Cu^{+} to Cu^{2+} at A-sites is associated with its migration from tetrahedral to octahedral sites below 300°C.

REFERENCES

1. B. Gillot, A. Rousset, *J. Solid State Chem.* **65,** 322 (1986).
2. B. Domenichini, B. Gillot, P. Tailhades, L. Bouet, and A. Rousset, *Solid State Ionics* **58,** 261 (1992).
3. B. Gillot, M. El Guendouzi, P. Tailhades, and A. Rousset, *React. Solids* **1,** 139 (1986).
4. P. Mollard, P. Tailhades, and A. Rousset, *IEEE Trans. Mag.* **26,** 241 (1990).
5. N. Nanba and S. Kobayashi, *Jpn. J. Appl. Phys.* **17,** 1819 (1978).
6. D. P. Seraphin, R. Lasky, and C. Y. Li, "Principles of Electronic Packaging." McGraw-Hill, New York, 1989.
7. S. Veprek, D. L. Cocke, S. Kehl, and H. R. Oswald, *J. Catal.* **100,** 250 (1986).
8. G. G. Jernigan and G. A. Somerjai, *J. Catal.* **147,** 567 (1994).
9. K. S. R. C. Murthy, S. Mahanty, and J. Ghose, *Mater. Res. Bull.* **22,** 1665 (1987).
10. X. X. Tang, A. Manthiram, and J. B. Goodenough, *J. Solid State Chem.* **79,** 250 (1989).
11. C. Vilette, P. Tailhades, and A. Rousset, *J. Solid State Chem.* **117,** 64 (1995).
12. C. Vilette, P. Tailhades, and A. Rousset, *C.R. Acad. Sci. Paris* **316**(série II), 1717 (1993).
13. T. Yamaguchi and T. Kimura, *J. Am. Ceram. Soc.* **59,** 333 (1976).
14. B. Gillot, F. Jemmali, and A. Rousset, *J. Solid State Chem.* **50,** 138 (1983).
15. C. Okasaki, *J. Phys. Soc. Jpn.* **15,** 2013 (1960).
16. M. Bhaduri, *J. Chem. Phys.* **75,** 3674 (1981).
17. E. Kitzinger and Z. Simsa, *Czech. J. Phys. B* **18,** 955 (1968).
18. L. Cervinka and Z. Simsa, *Czech. J. Phys. B* **20,** 470 (1970).
19. P. Poix, "Liaison Interatomiques of Propriétés Physiques des Composés Minéraux," p. 82. SEIDES, Paris, 1968.
20. P. Poix, F. Basile, and C. Djega-Mariadassou, *Ann. Chim. Fr.* **10,** 159 (1975).
21. S. S. Lisnyak, A. Ya Kesler, and D. Yu Tret'yakov, *Dokl. Akad. Nauk. SSSR* **297,** 1421 (1987).
22. J. Jarrige and J. Mexmain, *Bull. Soc. Chim. Fr.* **9–10,** 363 (1980).
23. B. Gillot, *J. Solid State Chem.* **113,** 163 (1994).
24. B. Gillot, F. Jemmali, L. Clerc, and A. Rousset, *React. Solids* **2,** 95 (1986).
25. B. Gillot, M. Kharroubi, R. Metz, R. Legros and A. Rousset, *J. Solid State Chem.* **91,** 375 (1991).
26. *Vibrational Spectrosc.* **6,** 127 (1994).
27. J. L. Verble, *Phys. Rev.* **B9,** 5236 (1974).
28. M. Lenglet, A. D'Huysser, J. Kasperek, J. P. Boulle, and J. Dürr, *Mater. Res. Bull.* **20,** 745 (1985).
29. J. Töpfer, A. Feltz, D. Gräf, B. Hackl, L. Raupach, and P. Weissbrodt, *Phys. Status Solidi A* **134,** 405 (1992).
30. A. D'Huysser, B. Lerebours-Hannoooyer, M. Lenglet, and J. P. Bonnelle, *J. Solid State Chem.* **39,** 246 (1981).
31. A. D'Huysser, A. Luchetti, G. Wrobel, and J. P. Bonnelle, *J. Microsc. Spectrosc. Electron* **2,** 609 (1977).
32. G. N. Kryukova, A. L. Chuvilin, and V. A. Sadykok, *J. Solid State Chem.* **89,** 208 (1990).
33. B. Gillot and M. El Guendouzi, *Mater. Chem. Phys.* **32,** 37 (1992).
34. M. J. Dreiling, *J. Phys. Chem. Solids* **37,** 121 (1976).
35. A. Navrotsky and O. J. Kleppa, *J. Inorg. Nuclear Chem.* **29,** 2701 (1967).
36. F. A. Kröger and H. J. Vink, in "Solid State Phyics," (F. Steitz and D. Turnbull, Eds.), p. 307. Academic Press, New York, 1956.
37. B. Gillot, B. Domenichini, and A. Rousset, *Ann. Chim. Fr.* **18,** 175 (1993).